Supporting information

High-Entropy Oxide Nanostructures for Rapid and Sustainable Nitrophenol Reduction

Anjali Varshney[a], Aishwery J. Verma[b], Ritesh Dubey[a], Sushil Kumar[a,*], Tapas Goswami[a,*], and Samar Layek[b,*]

[1]Department of Chemistry, Applied Science Cluster, School of Advanced Engineering, UPES, Dehradun, Uttarakhand 248007, India
[2]Department of Physics, Applied Science Cluster, School of Advanced Engineering, UPES, Dehradun, Uttarakhand 248007, India
* Corresponding authors: sushilvashisth@gmail.com, tapas.t@gmail.com, samarlayek@gmail.com

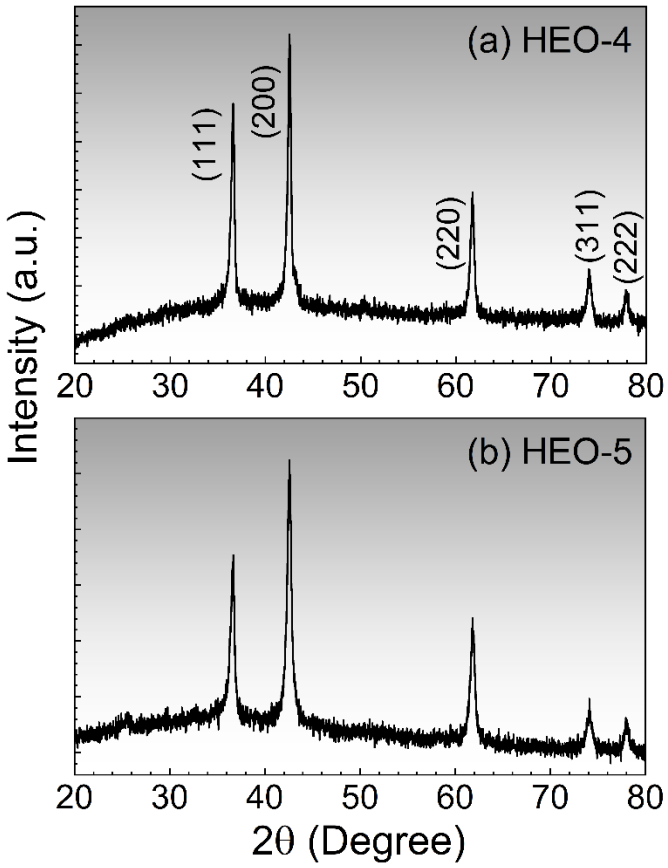

Fig. S1. Room temperature PXRD spectra for (a) **HEO-4** and (b) **HEO-5** nanostructures using Cu-Kα radiation.

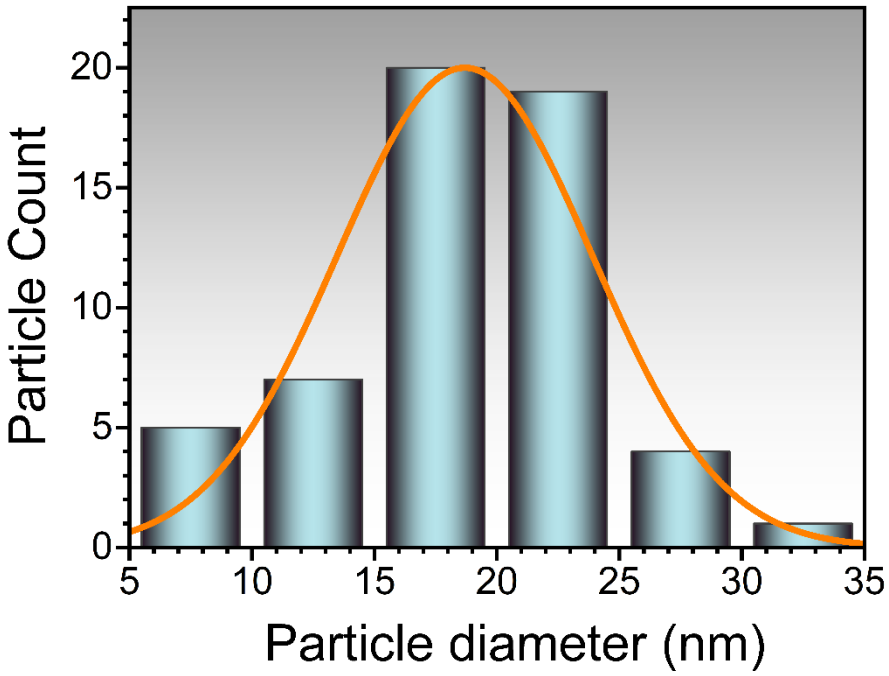

Fig. S2. Particle size distribution extracted from TEM image **HEO-5** nanostructures.

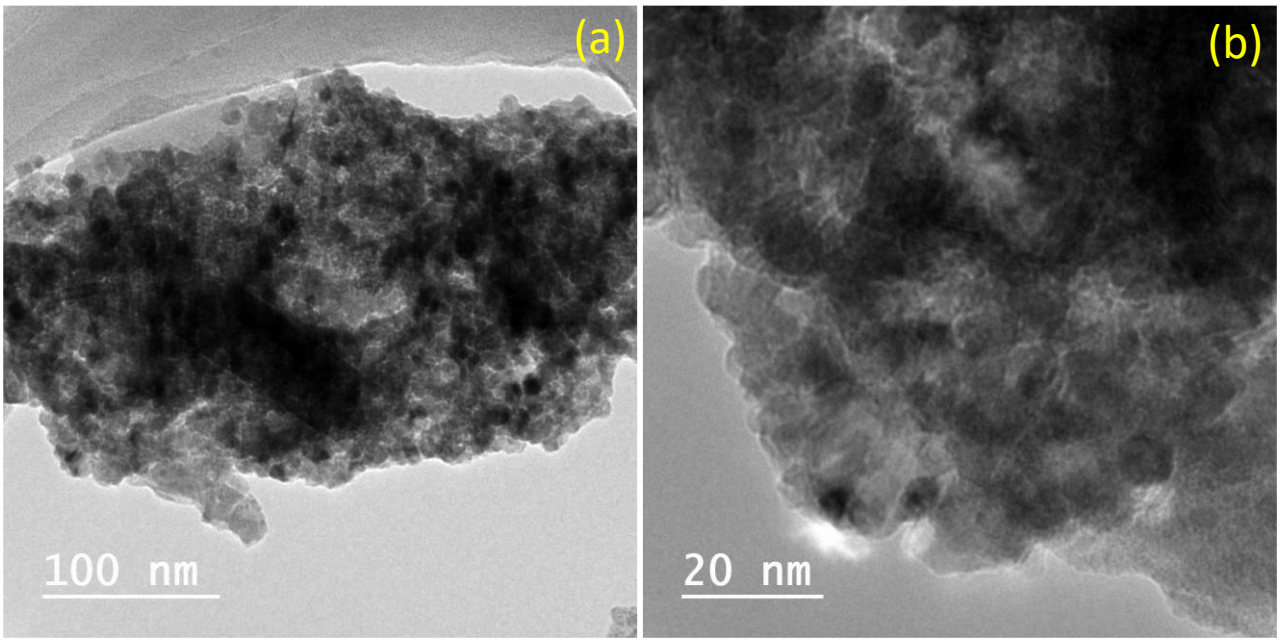

Fig. S3. (a-b) TEM micrograph for **HEO-4** nanostructures.

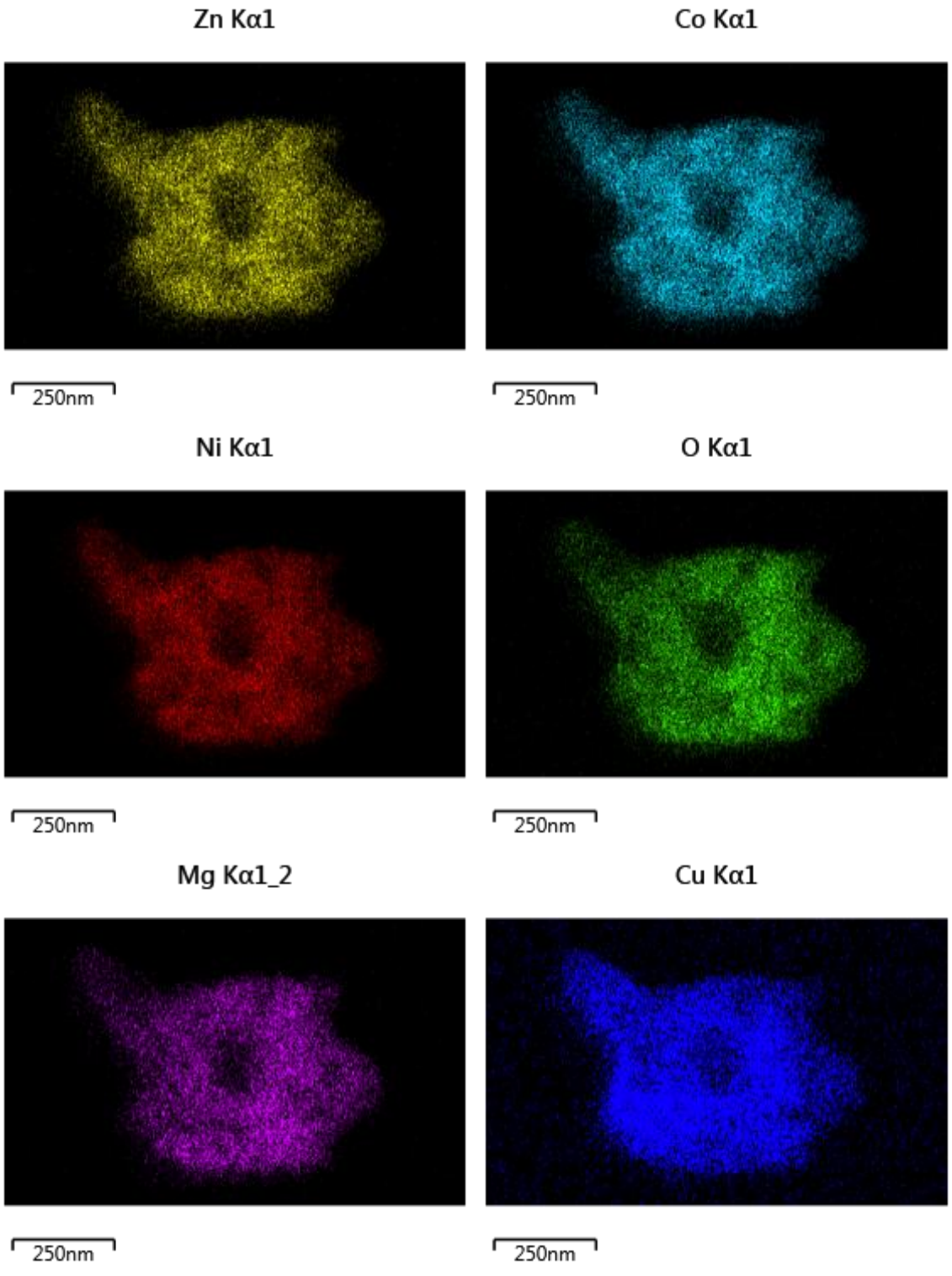

Fig. S4.TEM- EDS mapping of Zn, Co, Ni, O, Mg and Cu in **HEO-5** nanostructures.

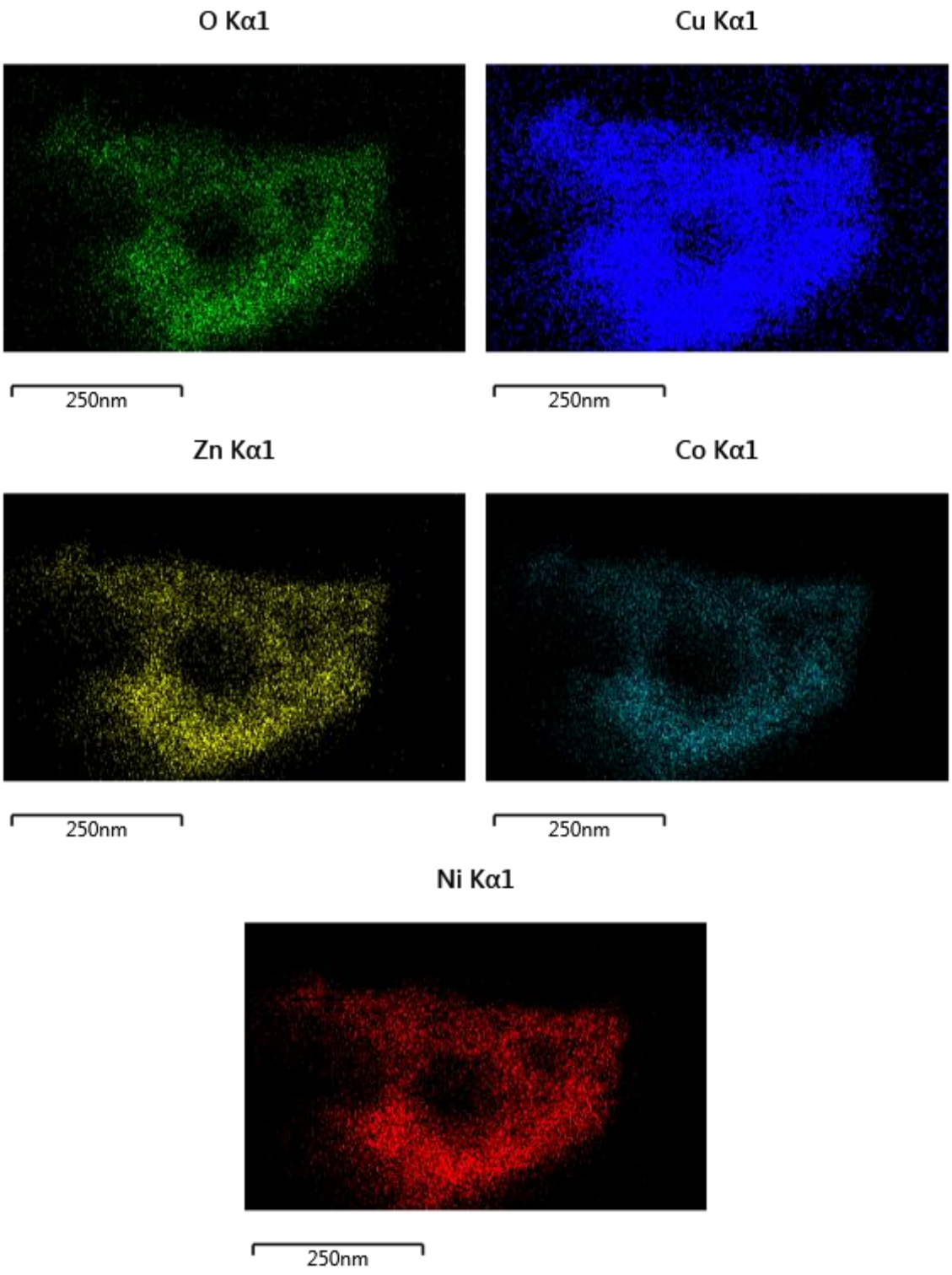

Fig. S5.TEM- EDS mapping of Zn, Co, Ni, O and Cu in **HEO-4** nanostructures.

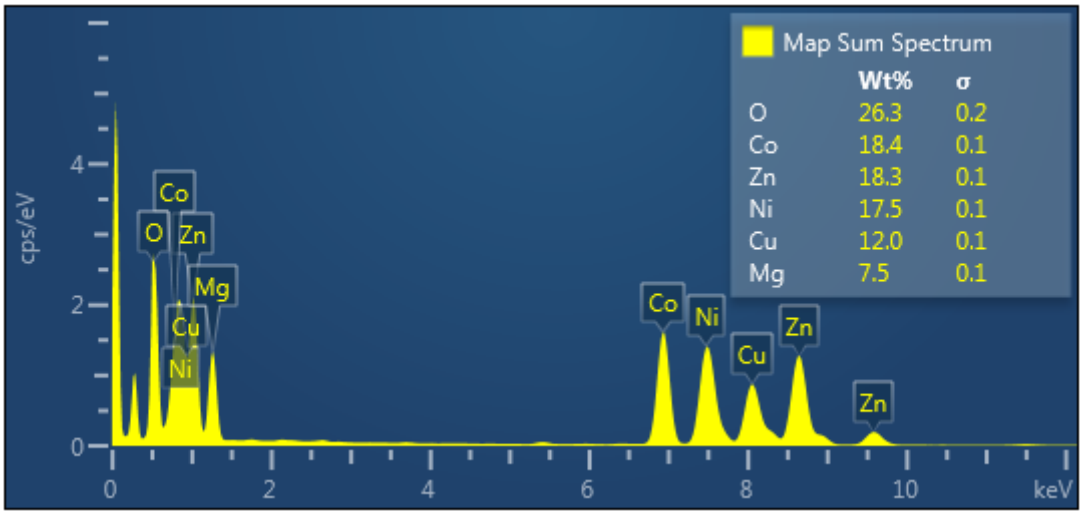

Fig. S6. TEM-EDAX spectra of **HEO-5**.

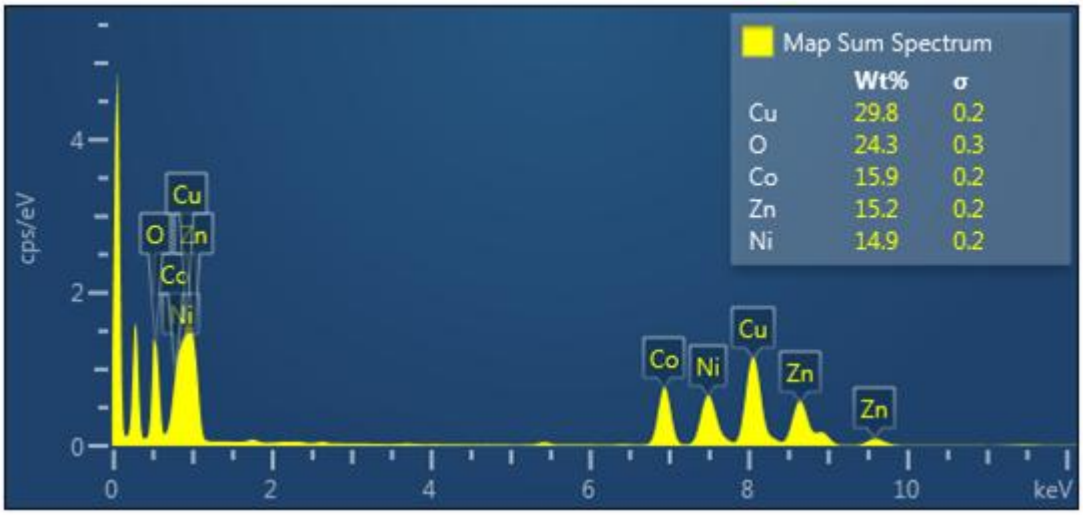

Fig. S7. TEM-EDAX spectra of **HEO-4**.

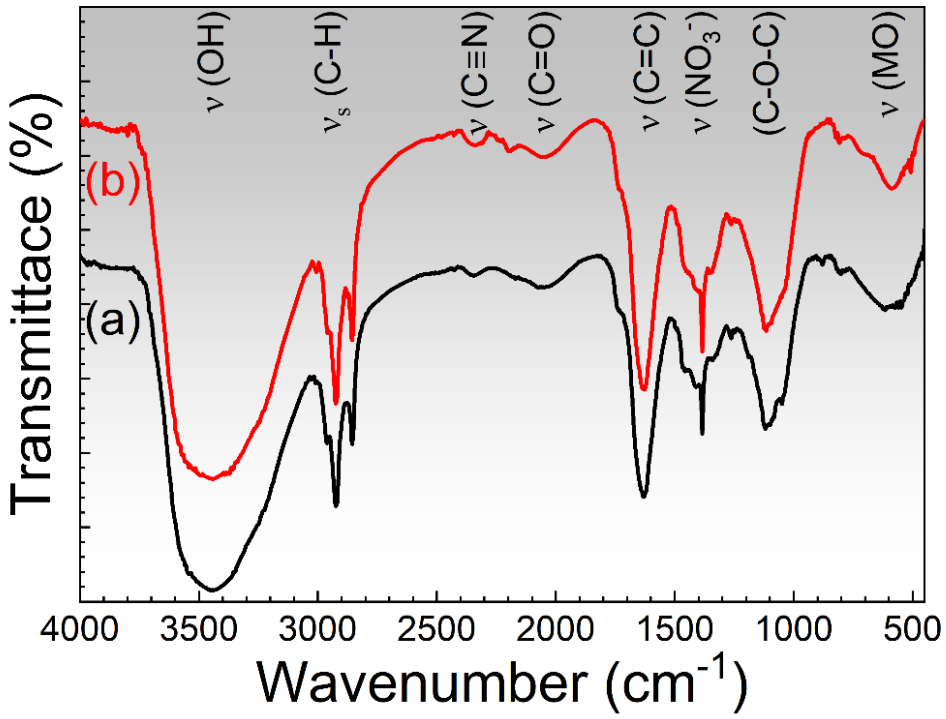

Fig. S8. Room temperature FTIR spectra of (a) **HEO-4** and (b) **HEO-5** nanostructures.

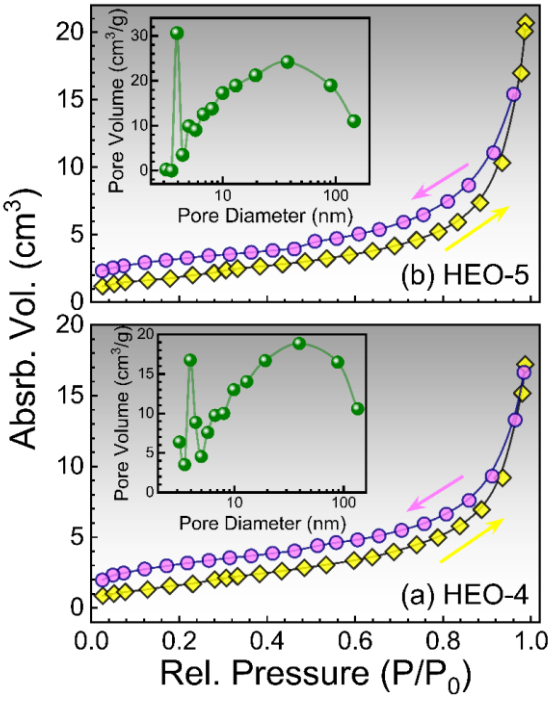

Fig. S9. BET nitrogen adsorption-desorption isotherms and pore size distribution plots (inset) of (a) **HEO-4** and (b) **HEO-5**.

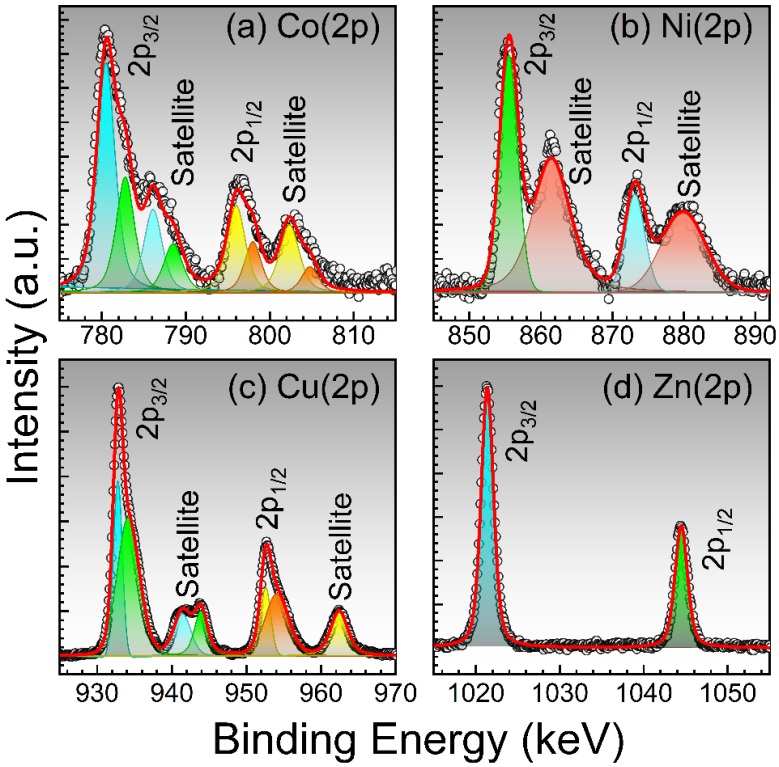

Fig. S10. Deconvoluted XPS spectra of (a) Co2p, (b) Ni2p, (c) Cu2p and (d) Zn2p for **HEO-4** nanostructures after background subtraction.

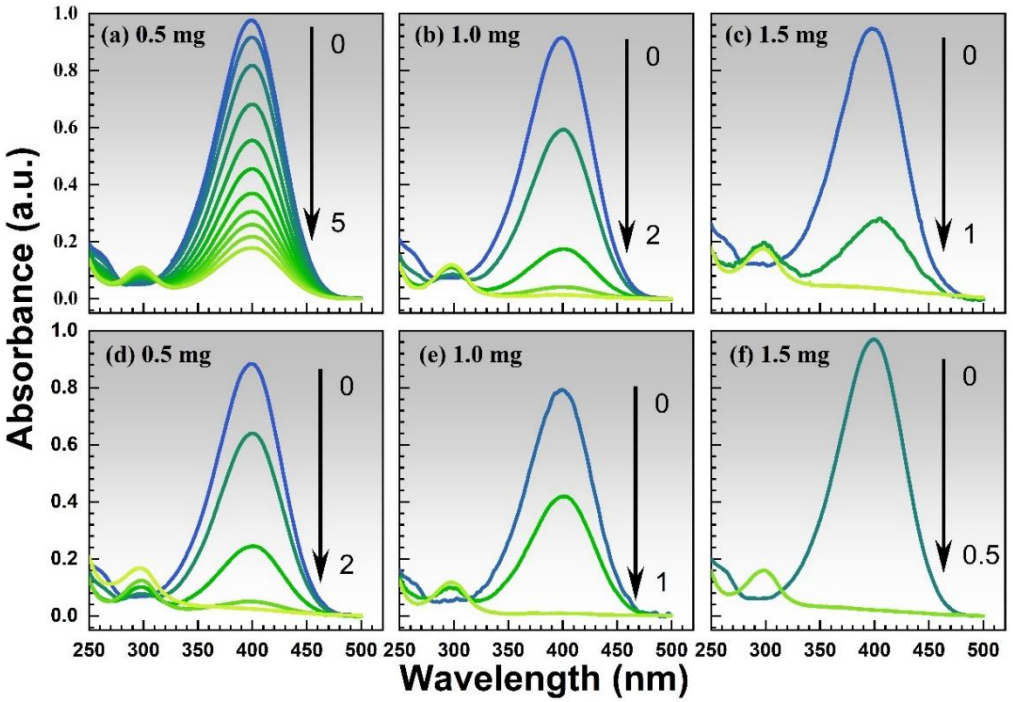

Fig. S11. UV-Vis spectral changes showing catalytic reduction of *p*-NP using 0.5, 1 and 1.5 mg of **HEO-4** (a-c) and **HEO-5** (d-f) catalysts respectively.

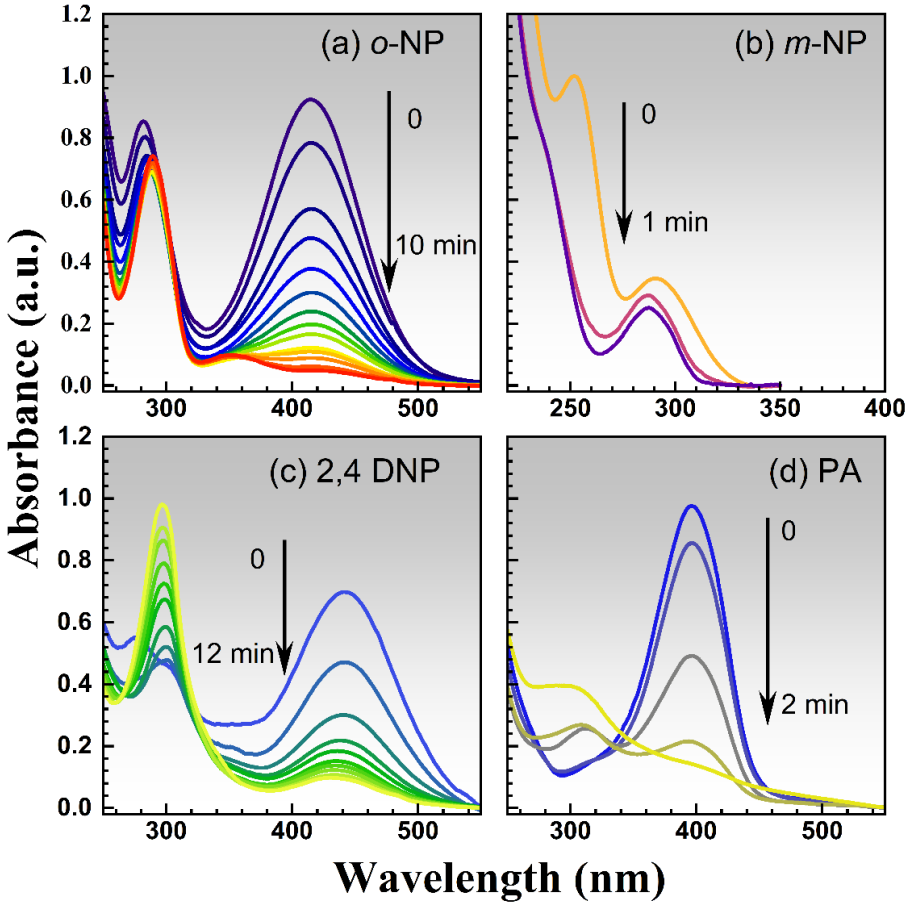

Fig. S12. Changes in the UV-Vis spectra showing catalytic reduction of (a) *o*-NP, (b) *m*-NP, (c) 2,4 DNP and (d) PA using 0.5 mg of **HEO-4** catalysts respectively.

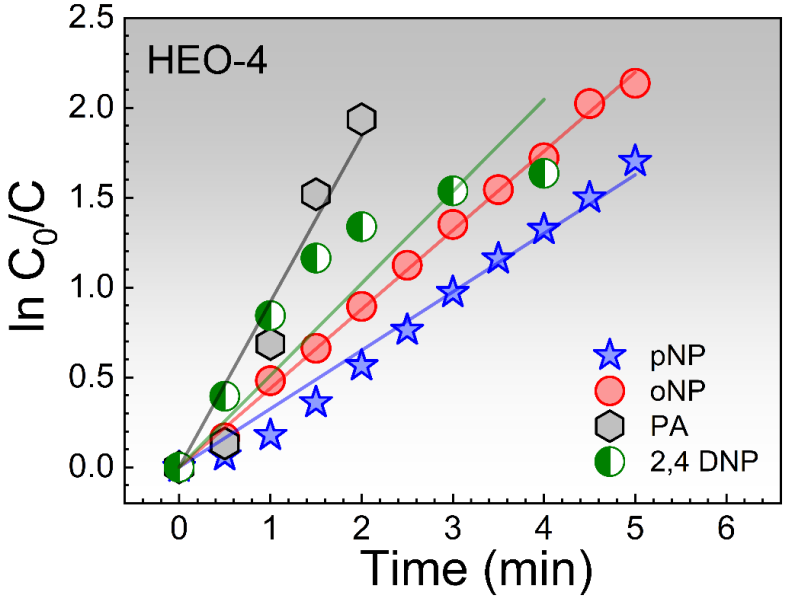

Fig. S13. Linear fit of ln(C_0/C) as a function of time for *p*-NP, *o*-NP, 2,4 DNP and PA using 0.5 mg of **HEO-4** catalysts.

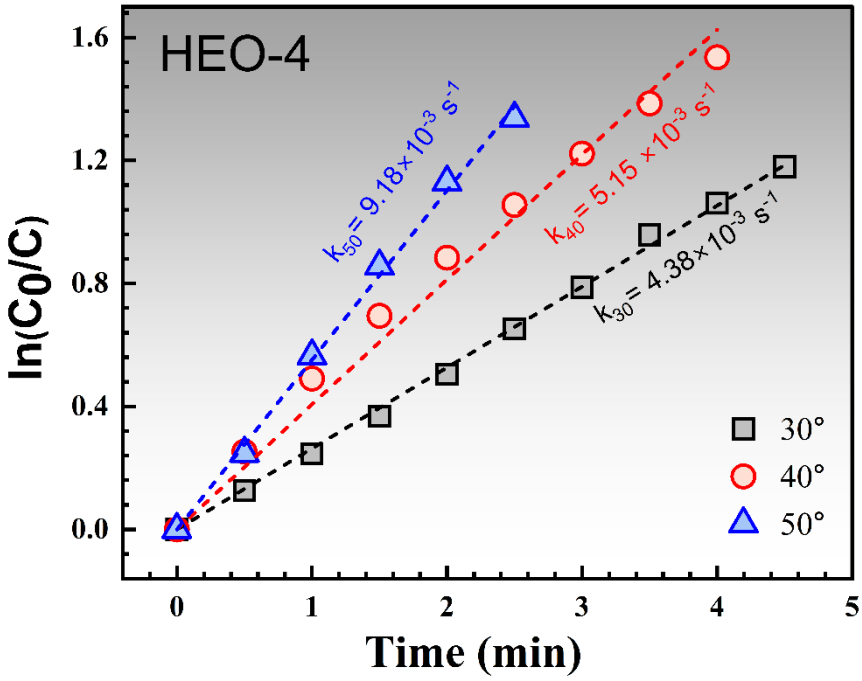

Fig. S14. Linear fit of ln(C_0/C) as a function of time for *p*-NP for different reaction temperatures (30º, 40º and 50º C) showing the value of rate constant using 0.5 mg of **HEO-4** catalysts.

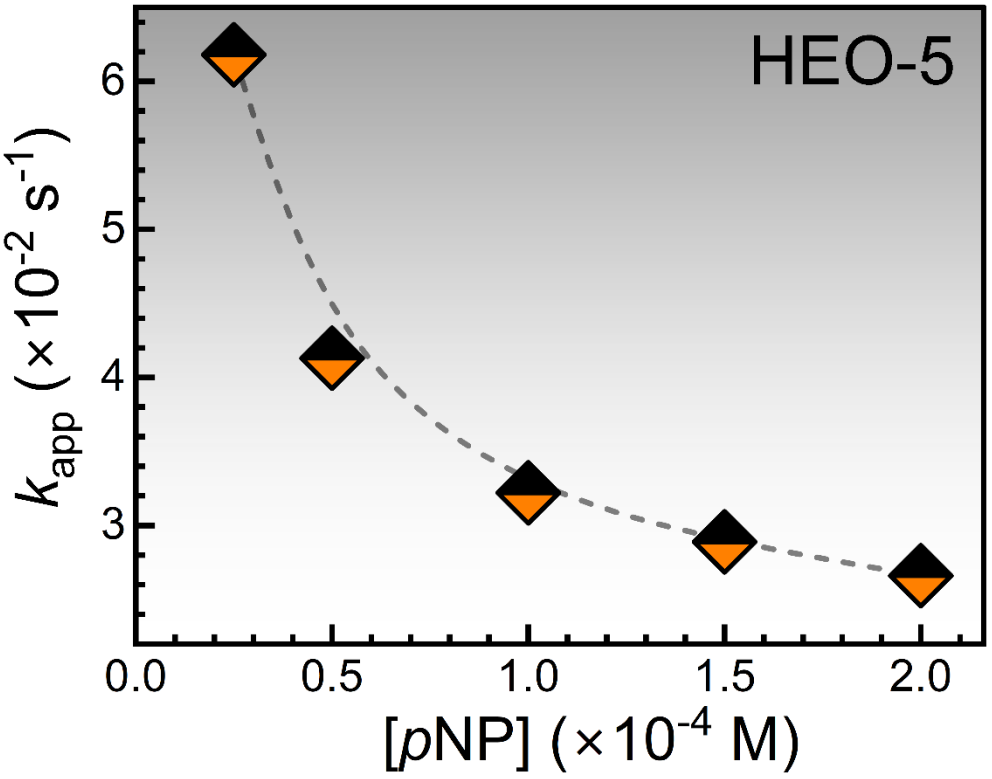

Fig. S15. Plot of rate constant (k_{app}) as a function of different amount of *p*-NP for **HEO-5** catalyst.

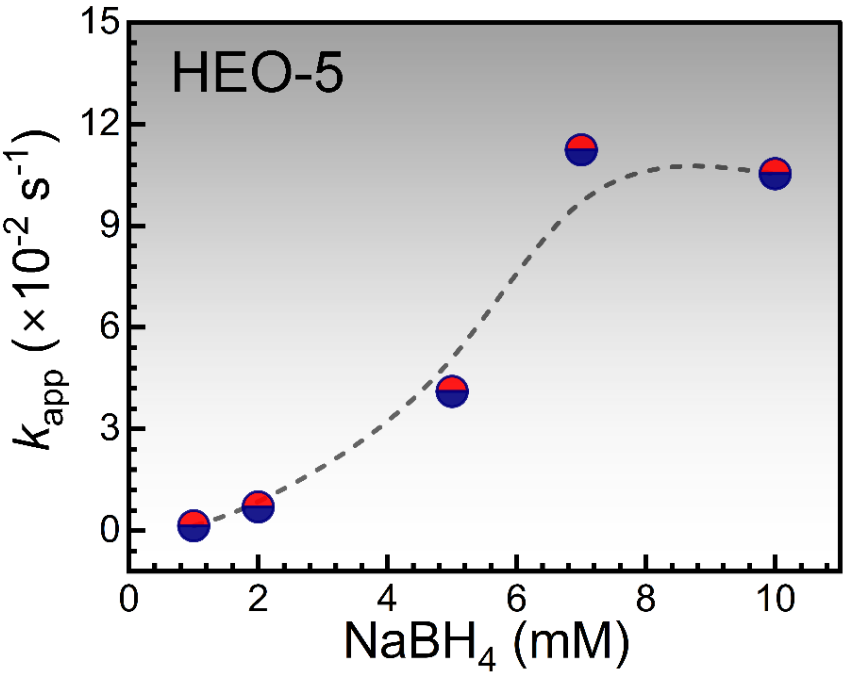

Fig. S16. Plot of rate constant (k_{app}) as a function of different amount of $NaBH_4$ for **HEO-5** catalyst.

Table S1. Comparison of catalytic *p*-NP reduction efficiency of **HEO-5** with the previously reported catalysts

Catalyst	Cat-loading (mg/mL)	[4-NP] (M)	t (min)	k(min^{-1})	References
SPION@Ni/Cu	1.0	0.005	1.16 min	0.103	[1]
NiO/CuO HNSs	0.0017	10^{-4}	3.3 min	1.5032	[2]
FeCoNb/NHC	1.0	10^{-4}	6 min	0.299	[3]
CuCoAl-LDH/rGO	2.5	0.02	1 min	2.952	[4]
PtRhCoNiMn NDHEA	1.0	10^{-4}	10 min	0.269	[5]
MoFeNi@np-AlFeNiCuPd	0.5	10^{-4}	2 min	2.314	[6]
CrMnFeCoNi (CMFCN-4)	10	1.4×10^{-3}	91 % in 30 min	0.17	[7]
AlCoCrFeNiV	1.1	1.6×10^{-3}	90 % in 30 min	0.0478	[8]
HEO-5	0.016	10^{-4}	0.5 min	1.932	**This work**

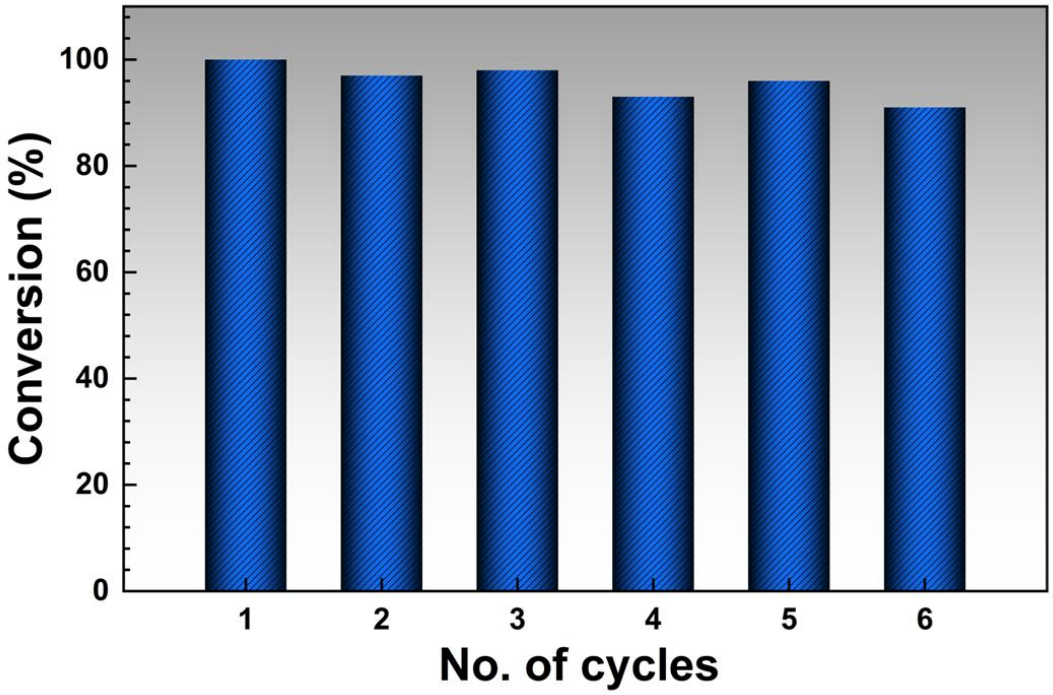

Fig. S17. Reusability studies performed by separating the catalyst from reaction mixture and reusing it for 6 cycles.

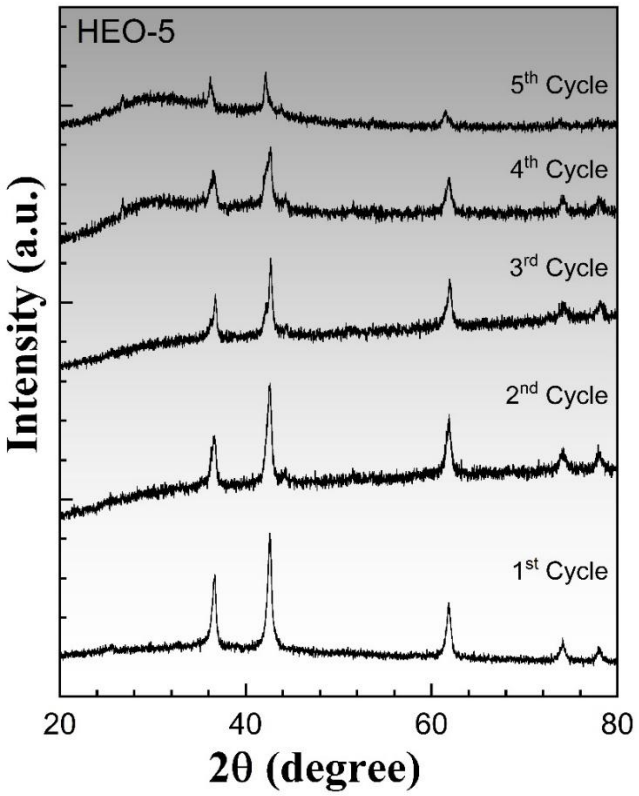

Fig. S18. PXRD pattern of **HEO-5** recovered from the reaction mixture after five reuse cycles.

Table S2. Thermodynamic parameters calculated from Eyring plots for the reduction of *p*-NP using **HEO-4** and **HEO-5** as catalyst.

Temperature (K)	$\Delta H^{\ddagger}$ (kJmol^{-1})		$\Delta G^{\ddagger}$ (kJmol^{-1})		$\Delta S^{\ddagger}$ (Jmol^{-1}K^{-1})	
	HEO-4	**HEO-5**	**HEO-4**	**HEO-5**	**HEO-4**	**HEO-5**
303	27.43	26.29	77.61	73.58	-165.4	-135.7
313			79.12	75.39	-164.9	-137.2
323			80.92	76.29	-165.4	-135.7

References

[1] A. Lourens, A. Falch and R. Malgas-Enus, *Mater. Chem. Phys.*, 2024, **315**, 129022.

[2] G. Wu, X. Liang, L. Zhang, Z. Tang, M. Al-Mamun, H. Zhao and X. Su, *ACS Appl. Mater. Interfaces*, 2017, **9**, 18207–18214.

[3] Z. F. Jiang, F. M. Tian, K. M. Fang, Z. G. Wang, L. Zhang, J. J. Feng and A. J. Wang, *J. Colloid Interface Sci.*, 2025, **677**, 718–728.

[4] D. Feng, Z. Wei, Q. Wang, A. Feng and H. Zhang, *ACS Appl. Mater. Interfaces*, 2022, **14**, 24265–24280.

[5] L. Zhang, Z. F. Jiang, Y. C. Shi, K. M. Fang, Z. G. Wang, J. J. Feng and A. J. Wang, *J. Colloid Interface Sci.*, 2025, **688**, 298–307.

[6] M. Peng, F. Wei, X. Li, J. Lan, M. Luo, Y. R. Lu and Y. Tan, *Sep. Purif. Technol.*, 2025, **357**, 130198.

[7] H. Peng, Y. Xie, Z. Xie, Y. Wu, W. Zhu, S. Liang and L. Wang, *J. Mater. Chem. A*, 2020, **8**, 18318–18326.

[8] Y. Kobayashi, D. Suzuki, S. Yokoyama and R. Shoji, *Int. J. Hydrogen Energy*, 2022, **47**, 3722–3732.